X-641-72-57
PREPRINT

THE APOLLO 15 X-RAY FLUORESCENCE EXPERIMENT

MARCH 1972

GODDARD SPACE FLIGHT CENTER
GREENBELT, MARYLAND

X-641-72-57

THE APOLLO 15 X-RAY FLUORESCENCE EXPERIMENT

I. Adler,[a†] J. Trombka,[a] J. Gerard,[ab] R. Schmadebeck,[a]
P. Lowman,[a] H. Blodget,[a] L. Yin,[a] E. Eller,[a] R. Lamothe,[a]
P. Gorenstein,[c] P. Bjorkholm,[c] B. Harris,[c] and H. Gursky[c]

I

March 1972

---

[a] NASA Goddard Space Flight Center.
[b] National Academy of Science.
[c] American Science and Engineering.
[†] Principal investigator.

ABSTRACT

The prime purpose of the X-ray fluorescence spectrometer carried in the Scientific Instrument Module (SIM) of the Command-Service Module (CSM) was to map the lunar surface with respect to its chemical composition. Results are presented for Al, Mg, and Si as Al/Si and Mg/Si ratios for the various features overflow by the spacecraft. The secondary purpose of the experiment was to make X-ray astronomical observations during transearth coast. The astonomical observations consisted of relatively long periods of X-ray measurements of pre-selected galactic sources such as Cygnus (Cyg X-1) and Scorpius (Sco X-1) and of the galactic poles. The lunar surface measurements involved observations of the intensity and characteristic energy distribution of the secondary or fluorescent X-rays produced by the interaction of solar X-rays with the lunar surface. The results showed that the highlands and maria are chemically different, with the highlands having considerably more Al and less Mg than the maria. The mare-highland contact is quite sharp and puts a limit on the amount of horizontal transport of material. The X-ray data suggests that the dominant rock type of the lunar highlands is a plagioclase rich pyroxene bearing rock probably anorthositic gabbro or feldspathic basalt. Thus the moon appears to have a widespread differentiated crust (the highlands) systematically richer in Al and lower in Mg than the maria. This crust is pre-mare and may represent the first major internal differentiation of the moon.

CONTENTS

ILLUSTRATIONS

ILLUSTRATIONS (Continued)

INTRODUCTION

In the experiment being described, the production of characteristic x-rays follows the interaction of solar X-rays with the lunar surface. The situation is summarized in Figure 1. Tabulated within the figure are the absorption edge energies E_k which are required to ionize the atoms in the K shell, and $E(K\alpha)$, the energies of the resulting characteristic X-ray lines. To produce the characteristic X-rays, an incident energy in excess of the binding energy of the electrons is necessary.

The results of numerous calculations indicate that the solar X-ray spectrum, typical of the sun's active regions is energetically capable of producing measureable amounts of characteristic X-rays from all the abundant elements with atomic number 14(Si) or less. During brief periods of more intense solar activity, excitation of higher atomic number elements will also occur.

The solar X-ray flux is known to vary on a time scale of minutes to hours. Thus, in the final analysis of the data, such features of the solar X-ray flux as intensity and spectral distribution must be considered in detail.

The solar X-ray flux, observed with low-resolution instruments such as proportional counters, decreases with increasing energy. If a strictly thermal mechanism of production is assumed, variable coronal temperatures are found to be somewhere between 10^6 to 10^7 °K. Such variations in temperature produce changes in both flux and spectral composition. In observing the lunar surface changes must be expected not only in fluorescent intensities but in the relative

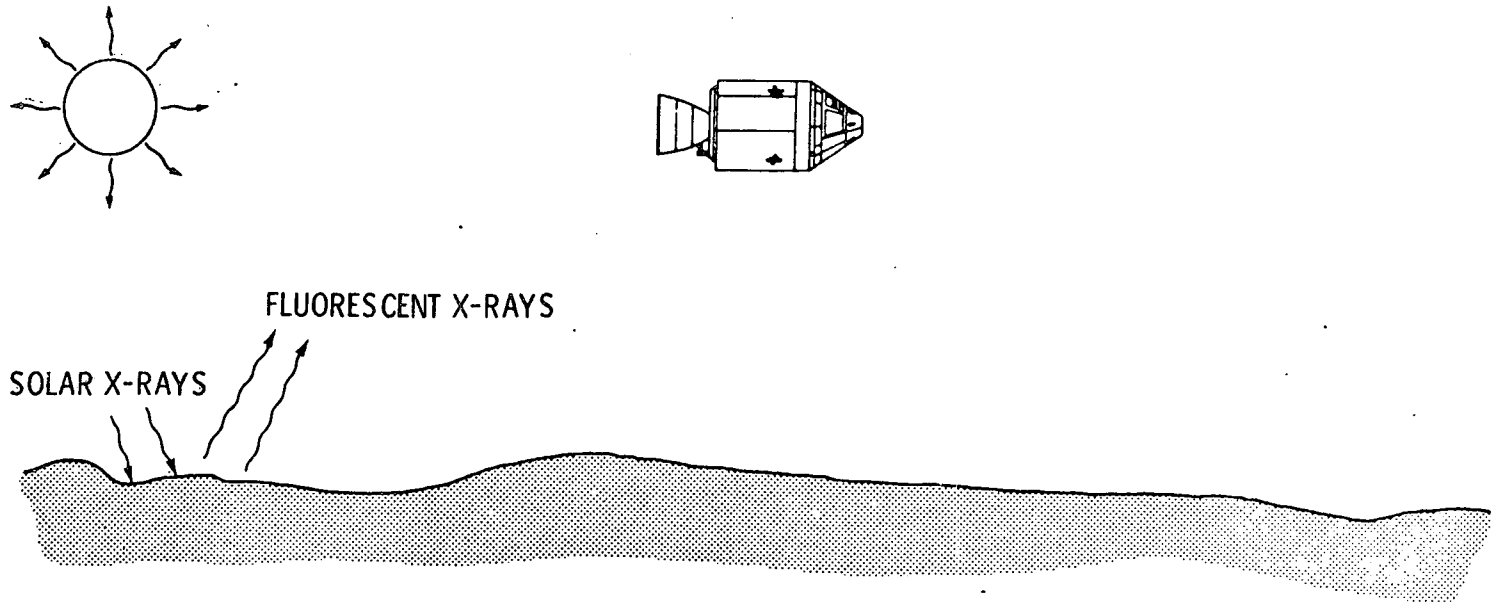

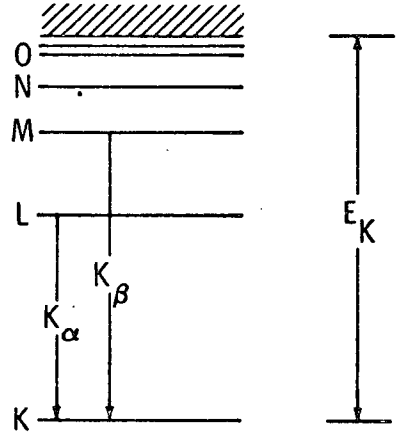

	$E(K_\alpha)$	ABSORPTION EDGES (E_k)
O	.54 KEV	
Fe	.73 KEV	
Na	1.04 KEV	
Mg	1.25 KEV	1.37 KEV
Al	1.49 KEV	1.57 KEV
Si	1.74 KEV	1.85 KEV
K	3.35 KEV	
Ca	3.70 KEV	

INNER ELECTRON TRANSITIONS GIVING
RISE TO CHARACTERISTIC K
X-RAY SPECTRA

Figure 1. X-Ray Fluorescence at Lunar Surface.

intensities from the various elements being observed. For example, if the solar spectrum hardens (larger fluxes of higher energies) or if there is an increase in solar characteristic line intensities on the high-energy side of the absorption edge of the heavier element, an enhancement of the intensities from the heavier elements relative to the lighter ones would be observed (see Figure 2).

An X-ray monitor was used to follow the possible variation in solar X-ray intensity and spectral shape. In addition, detailed simultaneous measurements of the solar X-ray spectrum were obtained in flight during the mission from the various Explorer satellites that measure solar radiation.

An estimated representative solar X-ray spectrum based on Solrad data taken during the flight period is shown in Figure 3. An attempt has been made to fit the observations with two temperatures, one for the quiet corona and the other for the more active regions. Superimposed on this curve along the energy axis are the K shell absorption edges for Mg, Al, Si, P and S. Only the solar X-rays with energies on the high side of the absorption edges are capable of exciting those elements and to a degree depending on the incident flux and ionization cross sections. Therefore, under quiet sun conditions, the solar flux is most suitable for exciting the light elements, including the major rock forming elements Si, Al and Mg.

DESCRIPTION OF THE INSTRUMENTATION

The instrumentation which has been described in detail elsewhere (Adler et al. (1972a)) will be only briefly described here.

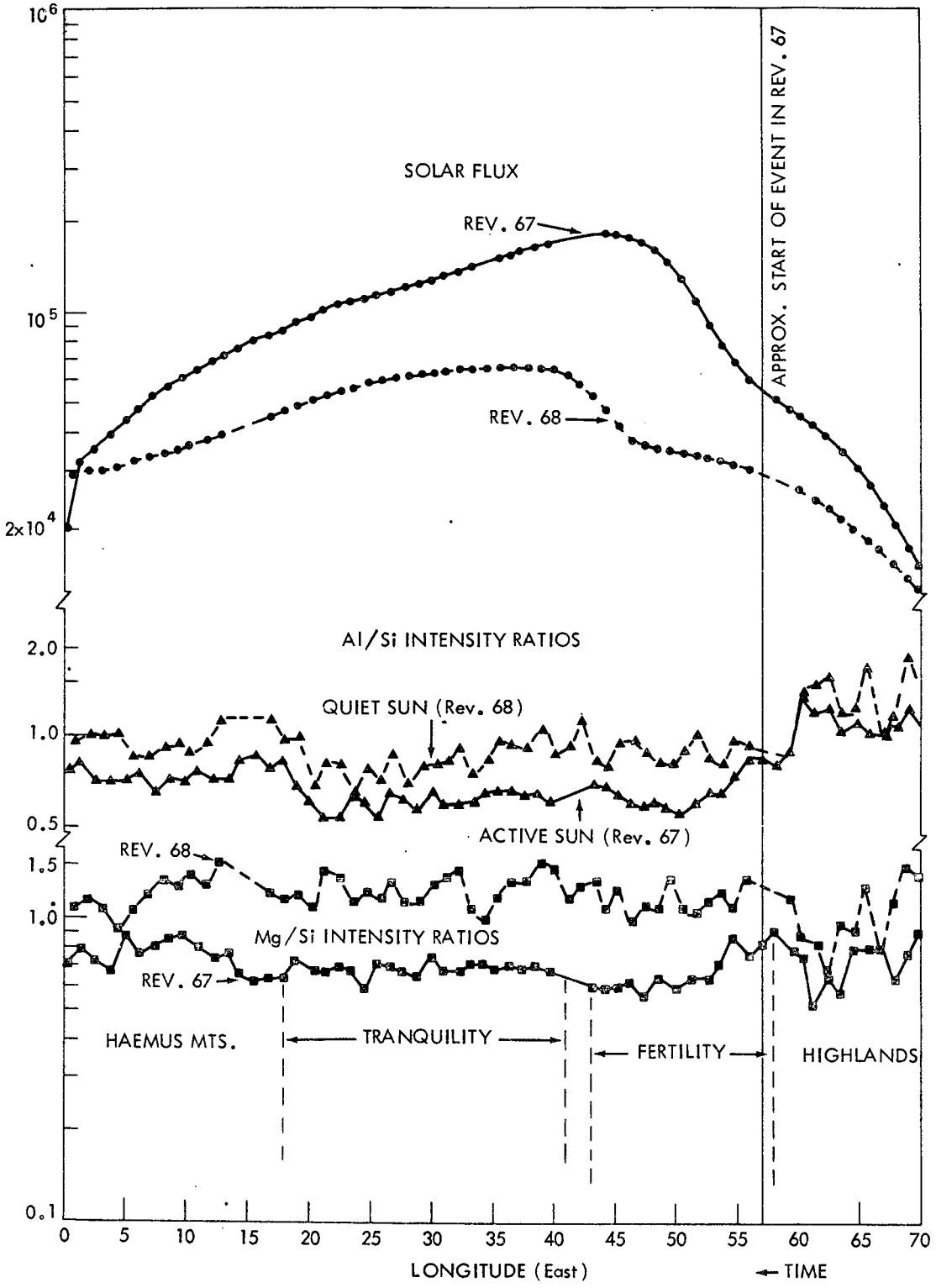

Figure 2. Al/Si and Mg/Si Intensity Ratios for Quiet and Active Sun Conditions

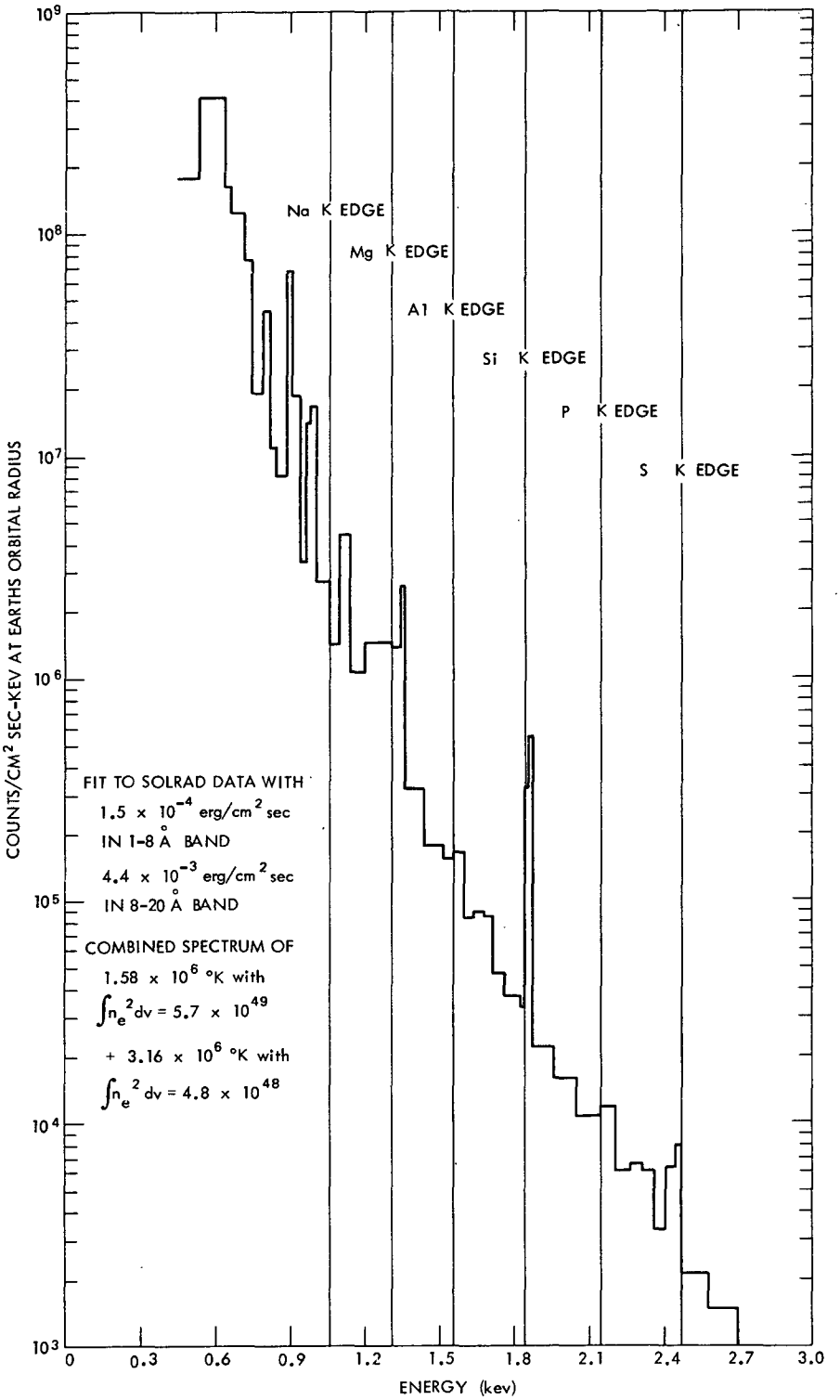

Figure 3. An Estimate of a Typical Quiet Sun X-Ray Spectrum

The X-ray fluorescence and alpha particle experiment is shown in functional configuration in Figure 4. The spectrometer consists of three main subsystems.

1. Three large area proportional counters that have state-of-the art energy resolution and 0.0025 cm thick beryllium (Be) windows.
2. A set of large area filters for energy discrimination among the characteristic X-rays of Al, Si and Mg.
3. A data handling system for count accumulation, sorting into eight pulse-height channels and finally, for relaying the data to the spacecraft telemetry.

The X-ray detector assembly consists of three proportional counters and two X-ray filters, mechanical collimators, an inflight calibration device, temperature monitors, and associated electronics. The detector assembly senses X-rays emitted from the lunar surface and converts them to voltage pulses proportional to their energies which are then processed in the X-ray processor assembly. Provisions for inflight calibration are made by means of programmed calibration sources, which, upon internal command, assume a position in front of the three detectors for calibration of gain, resolution and efficiency.

The three proportional counters are identical, each having an effective window area of approximately 25 cm^2. The window consists of 0.0025-cm-thick Be. The proportional counters are filled to a pressure of 1 atm with the standard P-10 mixture of 90 percent argon, 9.5 percent carbon dioxide, and 0.5 percent

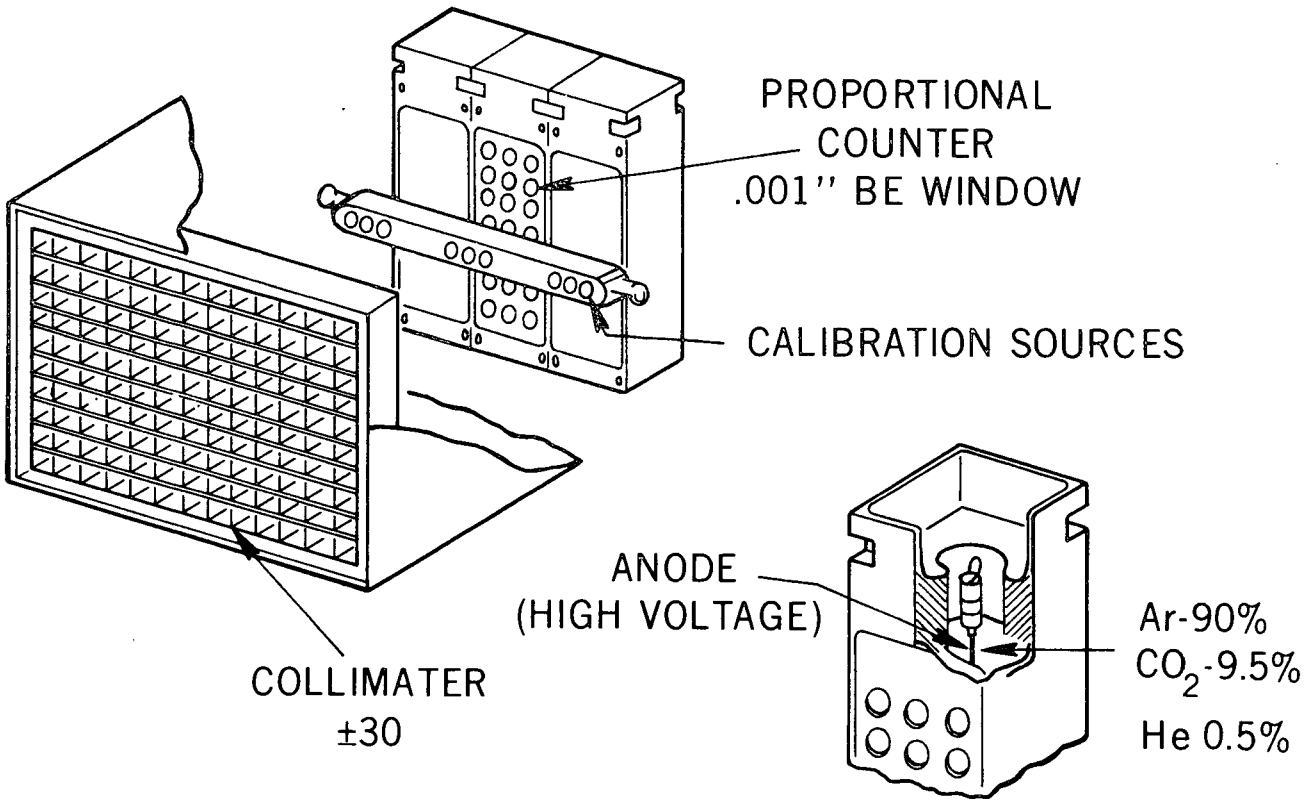

Figure 4. Functional Configuration of the X-Ray Spectrometer

helium. To change the wavelength response, filters are mounted across the Be window aperture on two of the proportional counters. The filters consist of a Mg foil and an Al foil 5.08×10^{-4} to 1.27×10^{-3} cm thick. The third counter does not contain a filter. A single collimator assembly is used to define the field of view (FOV) of the three proportional counters as a single unit. The collimator consists of multicellular baffles that combine a large sensitive area and high resolution but are restricted in FOV. The FOV determines the total flux recorded from the lunar surface and the spatial resolution. The FOV is specified as ±30° full width, half maximum (FWHM), in two perpendicular directions. The FWHM is the total angular width at which the collimator drops to one-half of its peak response. At the surface this translates into an instantaneous viewing area of 60 × 60 nautical miles at a spacecraft height of 60 nautical miles above the surface.

The inflight calibration device consists of a calibration rod with radioactive sources (Mg and Mn K radiation) that normally face away from the proportional counters. Upon internal command from the X-ray processor assembly, the rod is rotated 180° by a solenoid driver, thereby positioning the sources to face the proportional counters. Magnetically sensitive reed relays provide feedback signals indicating when the rod is fully in the calibration mode or fully in the noncalibration mode. These feedback signals are flag bits in the data telemetry output. The calibration command signal is generated in the X-ray processor assembly. The calibration cycle repeats every 16 min and continues for 64 sec.

In order to see higher energy radiation, should the sun be more active than anticipated, the bare detector (unfiltered) was programmed to operate in two modes, a high gain (normal) mode covering from about 0.75-2.75 kev and an alternate attenuated mode covering from 1.5-5.5 kev. During flight this detector alternately operates for 6 hours in the normal mode and 2 hours in the attenuate mode. The filtered detectors as well as the solar monitor continuously cover the energy range from 0.75-2.75 kev.

ANALYTICAL METHODS FOR DATA REDUCTION

The geochemical data reported below involving the ratios of magnesium and aluminum to silicon have been derived by an analysis of the pulse-height spectra observed with the three detectors. The following assumptions were made:

1. All three proportional counters have identical characteristics.
2. The detectors are 100% efficient for the radiation transmitted through the detector window.
3. All three detectors cover the same energy region (in the normal mode).

The intensity of X-rays observed in the three detectors are made up of the characteristic lines of the Si, Al and Mg, the scattered solar flux and background X-rays and high-energy radiation from various sources, galactic and otherwise. The methods of data reduction used were required to extract the characteristic line intensities from the total flux. This is summed up in the following expression:

$$G_i = \int_{.6\ \text{kev}}^{3.6\ \text{kev}} I(E)\ T_{Be}(E)\ F_i(E)\ \epsilon_i(E)\ dE$$

where

G_i is the total count in detector i where i = 1 is the bare detector,

i = 2 is the detector with the Mg filter and i = 3 is the detector with the Al filter.

$T_{Be}(E)$ is the X-ray transmission efficiency of the detector window as a function of energy. Since each detector has the same beryllium window (Be) and thickness, this transmission is independent of the detector.

$F_i(E)$ is the X-ray transmission efficiency of the filters as a function of energy.

$\epsilon_i(E)$ is the detector efficiency as a function of energy after the X-rays have been transmitted through the window. This is reasonably assumed as 100% for all the wavelengths in this energy range.

I (E) (as indicated above) consists of the characteristic lines, the scattered radiation and general background.

The background intensity was determined from measures on the dark side of the moon. The observations showed the background to be quite constant. Thus corrections could be simply made by subtracting these background values.

The problem of scatter was treated as follows: The scattered flux was divided into three energy regions covering the ranges 0.6 to 1.36 kev, 1.36 - 1.61

kev and 1.61 - 2.6 kev. Each interval was chosen to include the absorption edges of Mg, Al and Si respectively. Because of the nature of the solar spectrum the scattered flux in the region 1.36 - 2.6 is small compared to the fluorescence* (see Figure 3).

In the low energy region from 0.6 to 1.3 kev, if one combines the solar spectral distribution with the filtering effect of the Be window we get a transmitted energy distribution which has an average energy of about 1.2 kev, very close to the Mg Kα line. Thus one can consider the scattered energy in this region as being essentially monoenergetic and use the appropriate mass absorption coefficient. As a consequence, the calculated flux of X-rays in this region is a combination of scattered and fluorescent X-rays.

Thus the integral in equation (1) reduces to

$$G_i = \sum_{j=1}^{3} I_j^T T_j^{BE} Fi_j$$

I_j^T is the total X-ray flux at energy j where j is respectively the energy for the Mg, Al and Si K-lines, and where

$$I_j^T = I_j^C + I_j^S$$

I_j^C is the intensity of the characteristic line for energy j and I_j^S is the scattered intensity for the energy J

*The Al Si concentrations are high and most of the exciting energy is involved in photoelectric ionization.

$$I_2^S = I_3^S = 0$$

T_j^{BE} is the transmissions of the Be window for the energy j. F_{ij} is a filter factor for detector i and energy group j.

We thus have three simultaneous equations with three unknowns.

These equations can be solved by simple matrix inversion but we selected a least square inversion method which automatically calculates the statistical variance and covariance, the standard error due to counting statistics and background subtraction, and also to calculate interferences due to the fact that the filters are not ideal.

Furthermore an attempt has been made to arrive at actual concentration ratios for Al/Si. The approach to determining these concentrations is in part theoretical and in part empirical. The theoretical calculations are based on the assumption of a quiet sun and a coronal temperature of 4×10^6°K. These conditions give an X-ray energy distribution consisting of both a continuum and characteristic lines which is consistent with our solar monitor observations. Using this distribution and various compositions of soils as determined from the analysis of lunar samples we have been able to calculate a relationship between Al/Si and Mg/Si intensity ratios as a function of chemical concentration ratios.

Empirically, we have used soil values from the Apollo 11 site at Tranquility Base, Luna 16 values from Fecunditatis and Apollo 15 values from Palus Putredinus to be ground truth values (see Table 1). With these values and the

theoretically calculated slopes we have been able to determine the values of Al/Si concentrations and Mg/Si concentrations for various parts of the moon along the various ground tracks.

OPERATION OF THE EXPERIMENT

The X-ray experiment began to function 84 hr into the flight, during the third revolution around the Moon. From 84 to 102 hr ground elapsed time (GET), the orbit was approximately 8 by 60 n. mi. After 102 hr, the orbit was circularized and maintained at approximately 60 n. mi. until transearth coast. During the orbital period, more than 100 hr of surface measurements were made. The solar-monitor detector was used for simultaneous monitoring of solar X-ray flux. Lunar-far-side data were recorded on magnetic tape and telemetered on the near side. The data from the experiment were displayed in almost real time as numeric readout on a cathode ray tube monitor. The data were displayed in the form of running sums for the eight energy channels for each of the four detectors. The data obtained during the flight were used to plot compositional maps while the CSM was still orbiting the moon. These quick look values were for one minute integration intervals resulting in some degradation of spatial resolution (there is a 3 degree longitudinal displacement along the ground track due to the spacecraft motion). The prime data now being processed and reported here will be on the basis of 24 second integration intervals and a one degree surface displacement (60 $\times$ 80 sq. mile area).

As we have stated in the experiment description, the flux and energy distribution of the solar X-rays were expected to have a significant effect on the intensity of the fluorescent X-rays measured. This is very well demonstrated in Figure 2. Our solar monitor indicated increasing solar activity during part of orbit 67 as well as 73. The intensities for part of orbit 67 are compared to orbit 68 for the same longitudes (there was some small displacement of latitude). Also shown in this figure are Al/Si and Mg/Si intensity ratios. It can be seen that for the more active periods the Al/Si and Mg/Si ratios were depressed relative to the more normal orbit 68. This is due to a hardened solar X-ray spectrum which more efficiently excites the silicon relative to the aluminum and magnesium. This observation points out the great importance of monitoring the solar X-rays simultaneously with the surface X-rays. Figure 5 is a plot of the integrated intensities registered by the solar monitor for the approximate period corresponding to the surface measurements. These values were taken at the sub-solar point. Also shown are the corresponding surface measurements. With the exception of such orbits as 67 and 73, the solar flux was fairly stable, varying less than ± 30 percent of the mean value. This stability was likewise reflected in the surface data, which indicate a relatively stable incident flux as well as a stable spectral distribution.

OBSERVATIONS

This report is based on the reduction of data recorded on the prime mission tapes. There are thousands of data points based on twenty four second integration

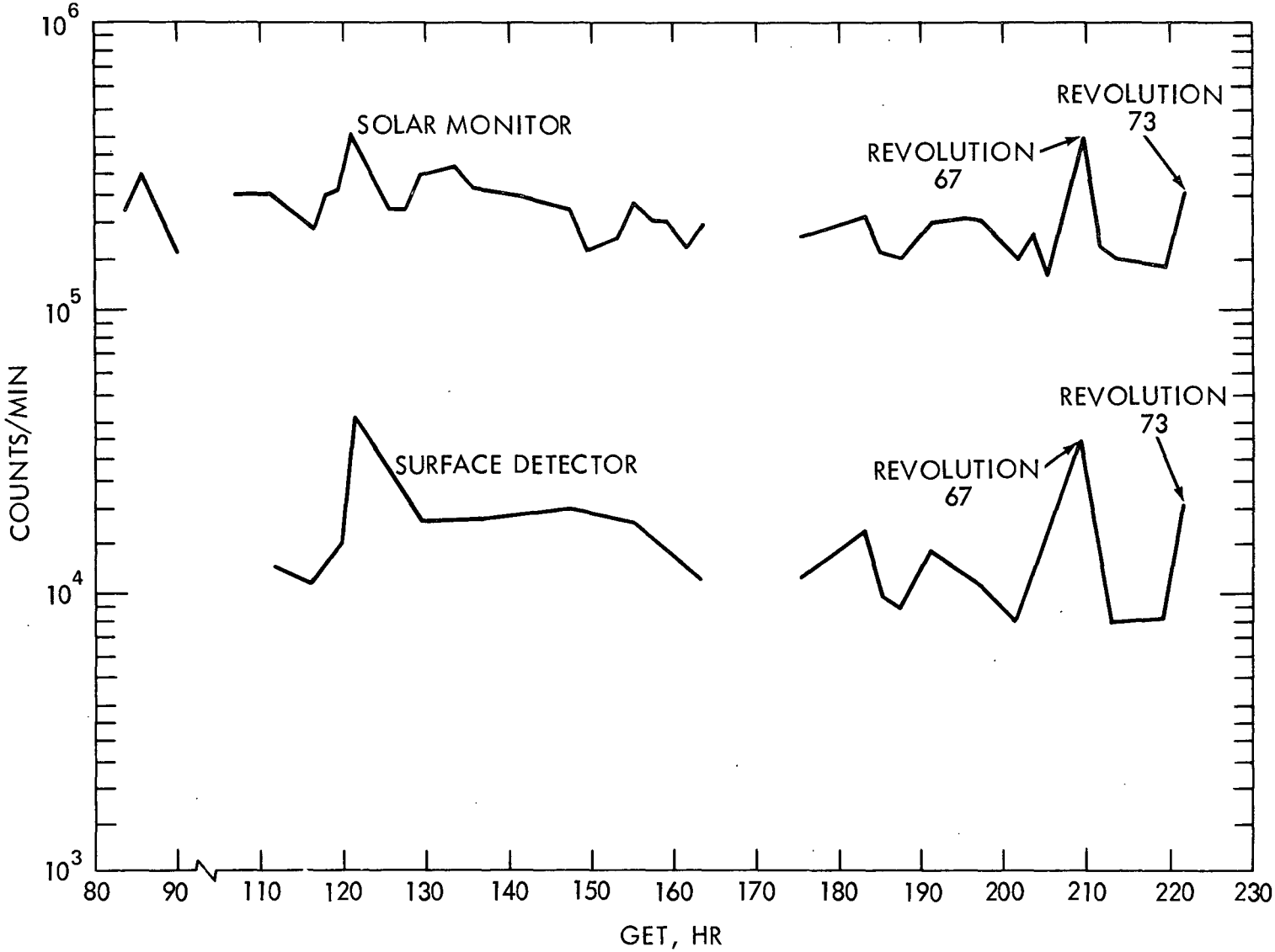

Figure 5. Integrated Intensities Registered by the Solar Monitor for the Approximate Period Corresponding to the Surface Measurements

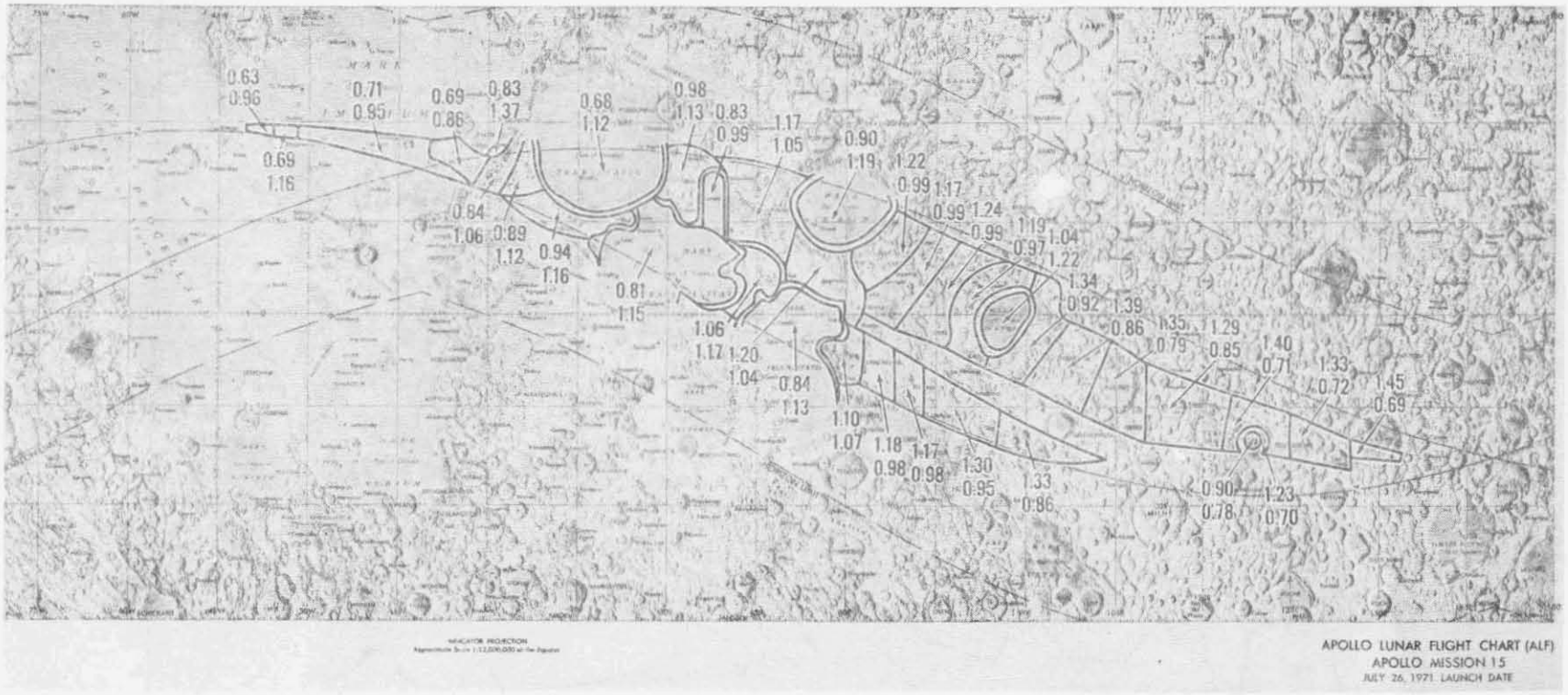

Figure 6. Al/Si and Mg/Si Intensity Ratios for Specific Areas along the Apollo 15 Groundtracks (The upper values are Al/Si and the lower values are the Mg/Si.)

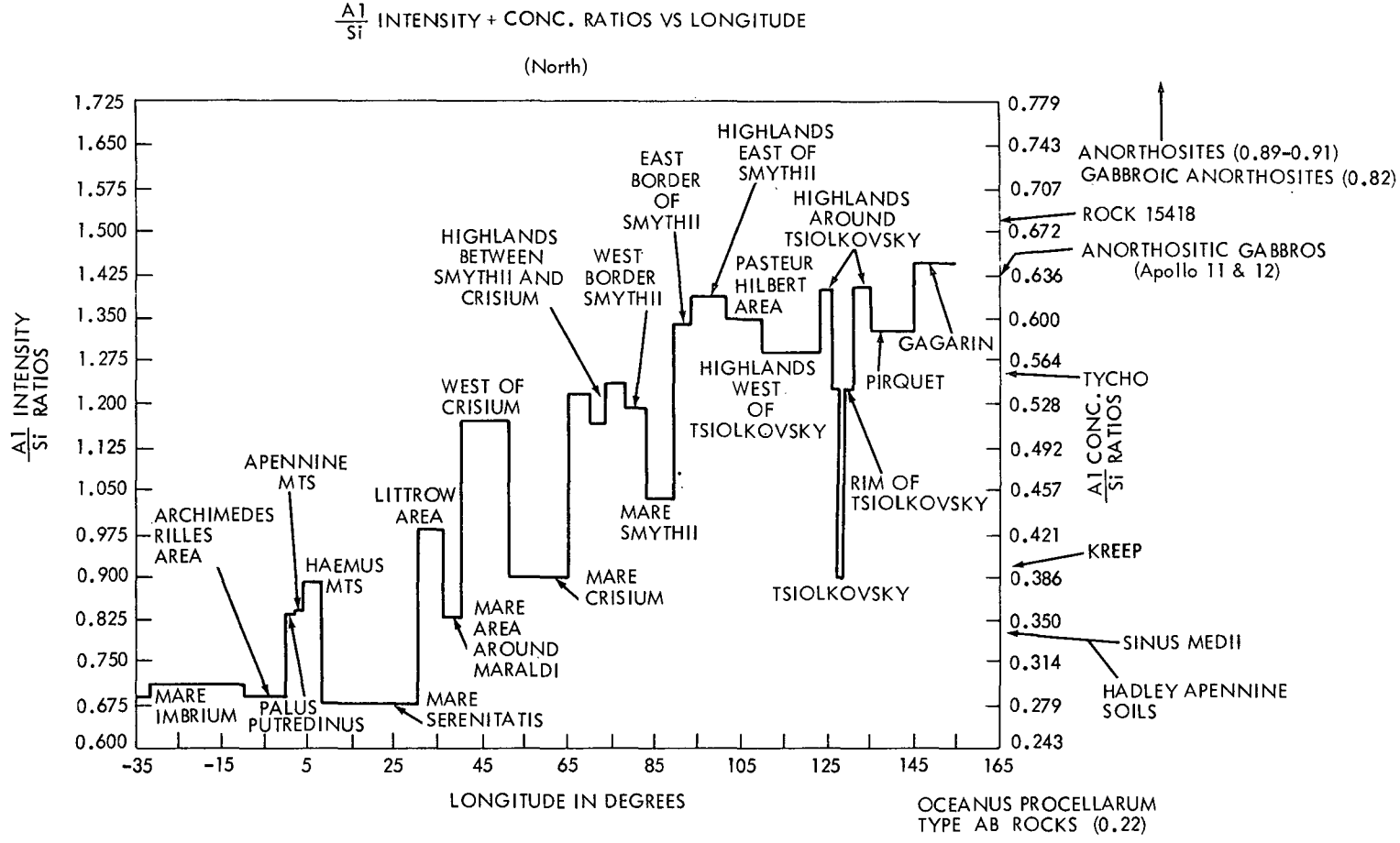

Figure 7a. Al/Si Ratios for a Northerly Track

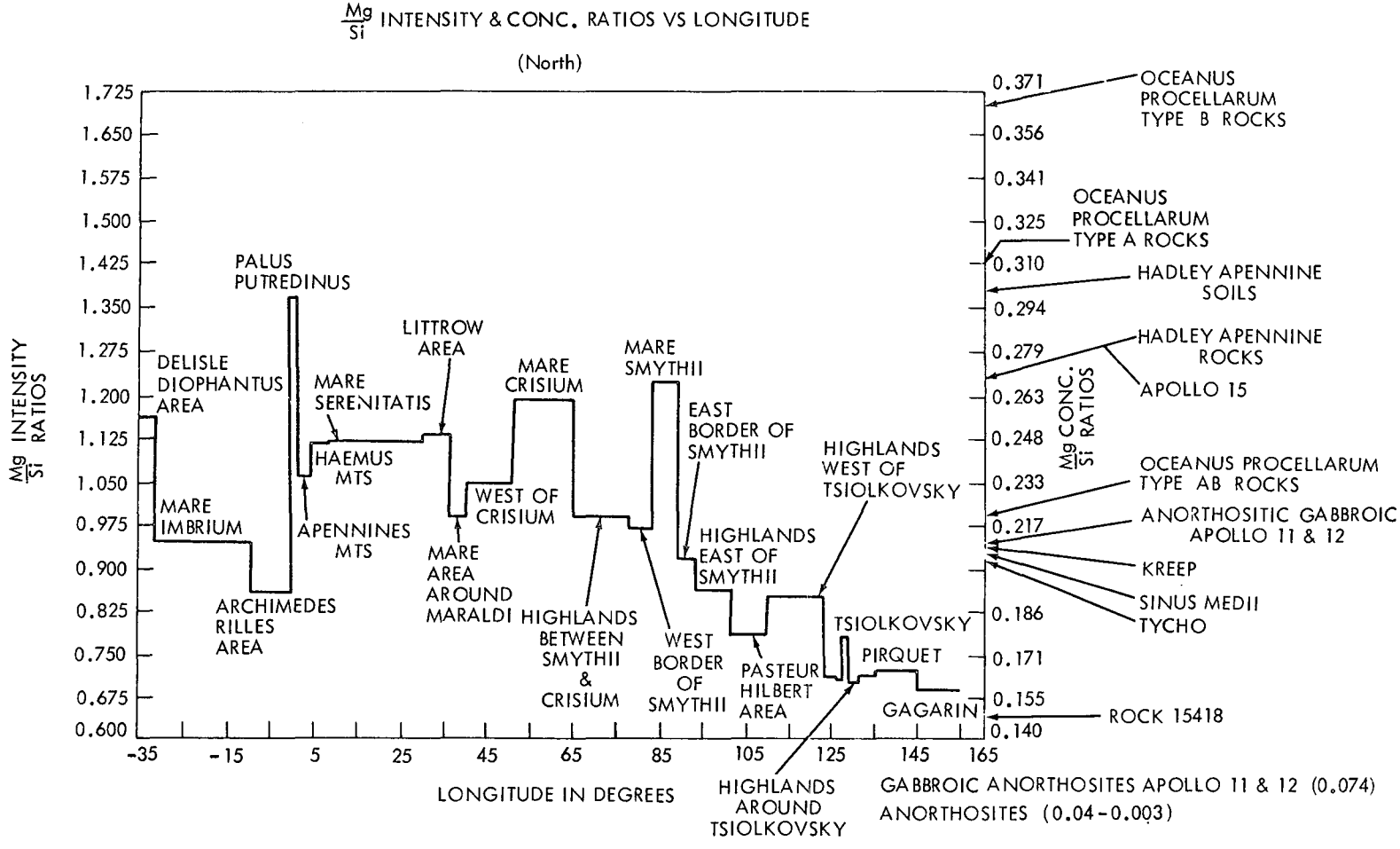

Figure 7b. Mg/Si Ratios for a Northerly Track

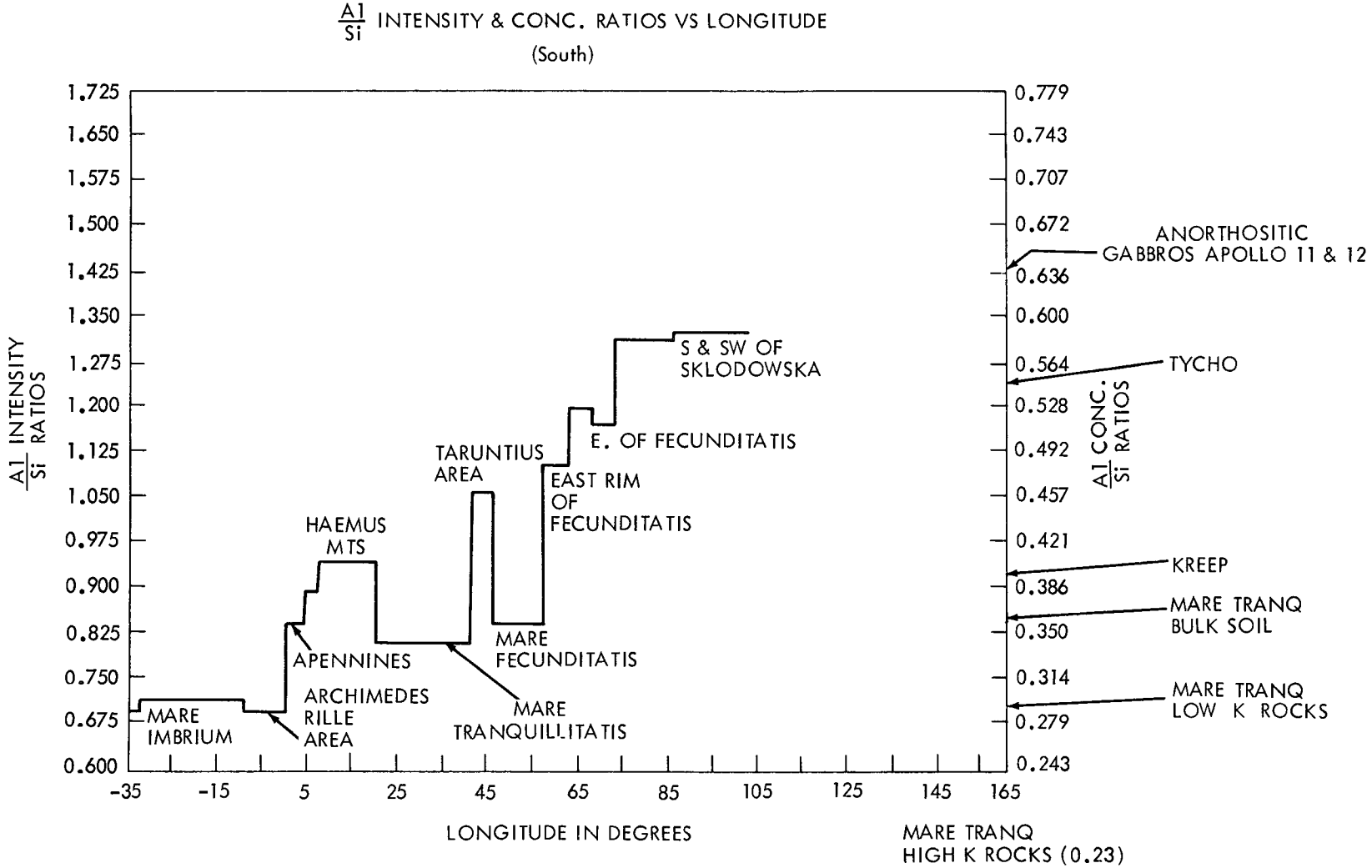

Figure 8a. Al/Si Ratios for a Southerly Track

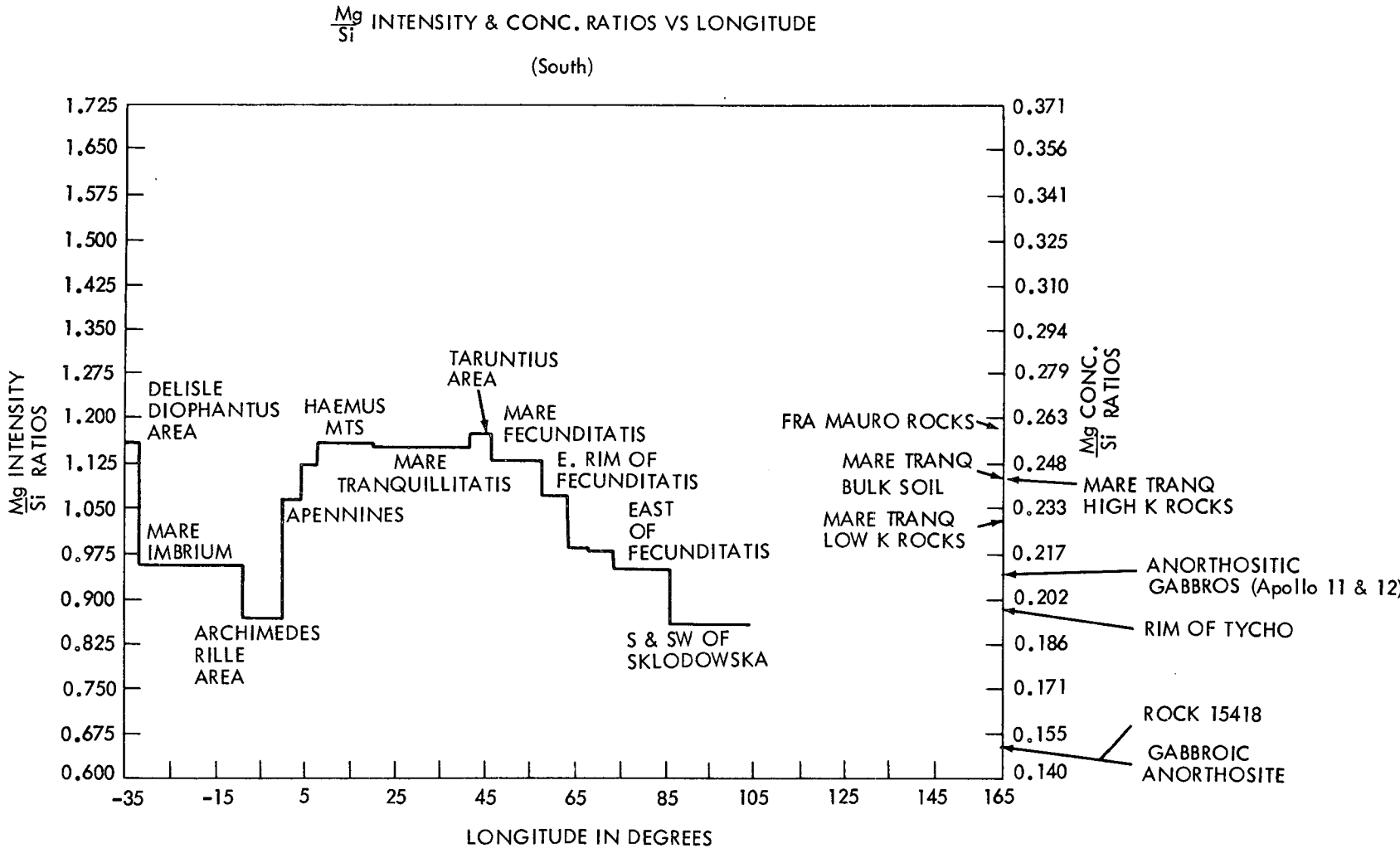

Figure 8b. Mg/Si Ratios for a Southerly Track

times. Most of the time we will be using intensity ratios rather than concentrations for convenience sake, however these values just as effectively indicate important trends. The data presented here include Al/Si and Mg/Si relationships to terrain and returned lunar samples. The X-ray experiment provided data from that part of the lunar ground track illuminated by the sun. An examination of the ground tracks from east to west indicates that the spacecraft passed over such features as the craters Gagarin, Tsiolkovsky, the far side and eastern limb highlands, the mare areas such as Smythii, Crisium, Fecunditatis, Tranquillitatis, Serenitatis, Imbrium and Oceanus Procellarum, and Haemus mountains and the Apennines. The Al/Si intensity ratios varied by more than a factor of 2 between the eastern limb highlands and the mare areas. The Mg/Si intensity ratios varied by about a factor of 2. The situation is clearly shown in Figure 6. The part of the moon that was overflown has been divided into a number of areas some representing distinct lunar features. The upper figures in each segment are Al/Si and the lower figures are Mg/Si intensity ratios. These values are averages, taken from a substantial number of ground tracks. The situation is further detailed in Table 1. Where N is the number of individual data points used to calculate the averages. The table further indicates the scatter of observed values for each feature. Figures 7 and 8 show the Al/Si and Mg/Si intensity ratios and concentration ratios for north and south tracks vs. longitude. In addition the right hand side of the figures shows the Al/Si and Mg/Si concentration ratios of selected lunar samples for reference.

The following observations can be drawn:

1. The Al/Si intensity values are lowest over the mare areas and highest over the non-mare areas. The extremes vary from about 0.63 in Imbrium to 1.45 near Gagarin. The Mg/Si ratios tend to be lowest in the highlands and highest in the Mare areas. The Mg/Si intensity ratios vary from about 0.69 at Gagarian to about 1.4 in Palus Putredinus.
2. The Al/Si values for the Apennines and Haemus mountains is about 0.9, intermediate between Imbrium and the eastern limb highlands. On the other side of the Apennine mountains in the Archimedes Rille area, the observed values is about 0.70.
3. An examination of the Al/Si coordinate plot shows that the values tend to increase from the western mare areas to the eastern limb highlands.

An interesting correlation has been observed between Al/Si ratios and optical albedo values as is shown in Figures 9 and 10. Generally, higher Al/Si ratios correspond to higher albedo values. There are occasional deviations from this relationship caused by surface features. The composition of areas with different albedos can be inferred by using the X-ray data. It is possible, for example, to state whether albedo variations are related to chemical differences or to the nature and, perhaps, age of a given feature.

GEOLOGIC INTERPRETATION

The x-ray data provide considerable insight to the moon's geology, when viewed in the context of returned sample analysis and the other orbital science

experiments. The following interpretations are considerably more specific than those previously published (Adler et al, (1972b)). However, they are still subject to revision; it should be stressed that although a wide range of lunar terrain was covered, the area for which we have data is less than 15% of the moon's total surface.

The most general conclusion from the measured x-ray intensities and shown above is that the highlands and maria are chemically different, with the highlands having considerably more aluminum and less magnesium than the maria. These differences, and the sharpness of the mare/highland contact shown by changes in x-ray intensity, argue against the theory that the maria are essentially dust eroded from the highlands (Gold (1966)) and electrostatically transported horizontally to low spots. Such a process would tend to obliterate original chemical contacts, and there is no obvious reason why it should produce chemical differentiation between highlands and maria. Further evidence against the dust theory in which the supposed absence of far-side mare material is explained by the fact that the far side is shielded from the earth's magnetic tail, (Gold (1972)) is provided by the evidence for a mare-like composition of the dark material in the floor of Tsiolkovsky. The relative freshness of the surrounding ejecta blanket indicates that this crater is probably Eratosthenian in age, and probably formed after the moon's rotation became locked; thus it can not be argued that the far side was exposed to the earth's magnetic tail when Tsiolkovsky was filled.

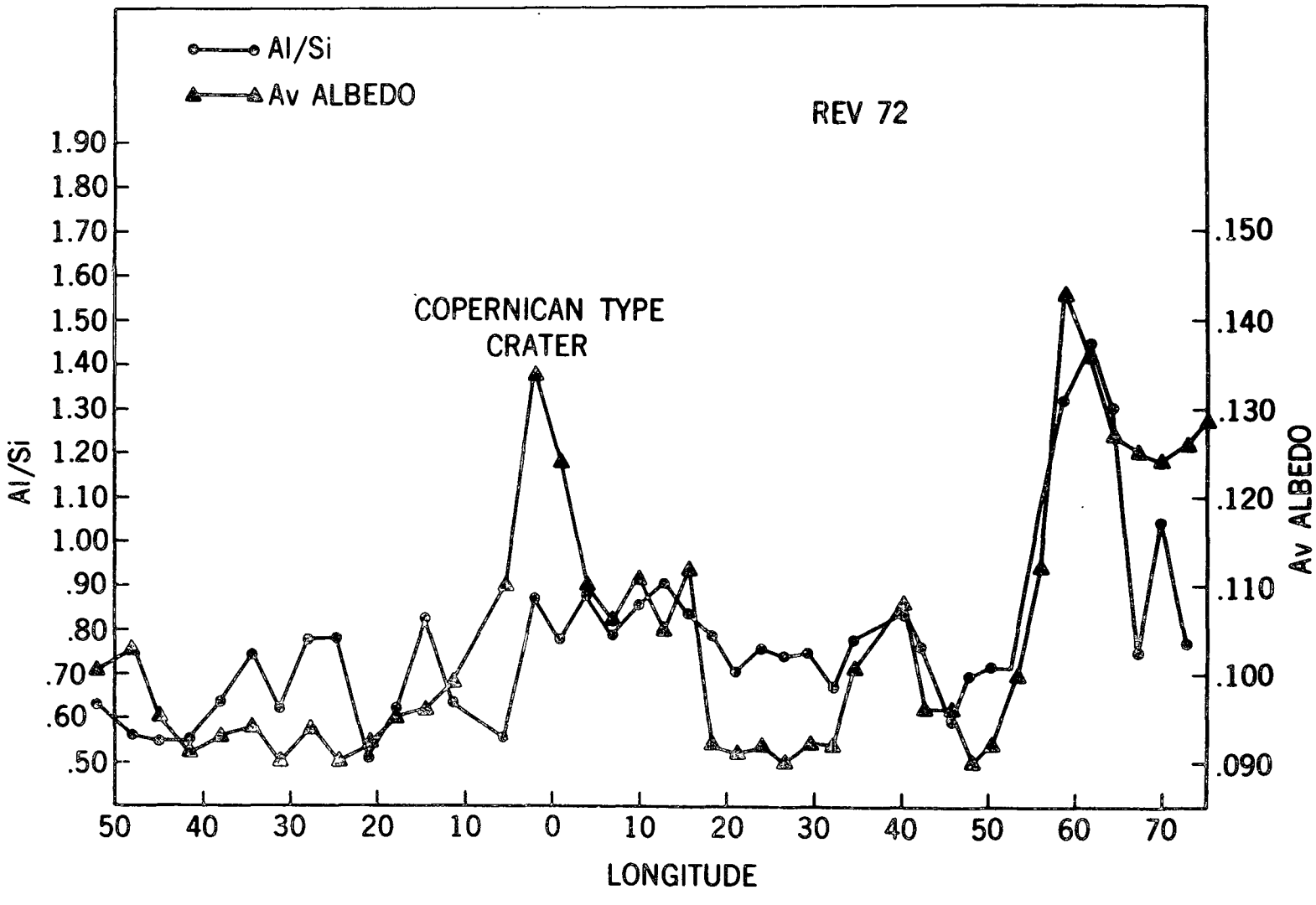

Figure 9. Intensity Ratios Compared to Optical Albedos along the Ground Track Corresponding to Orbit 25

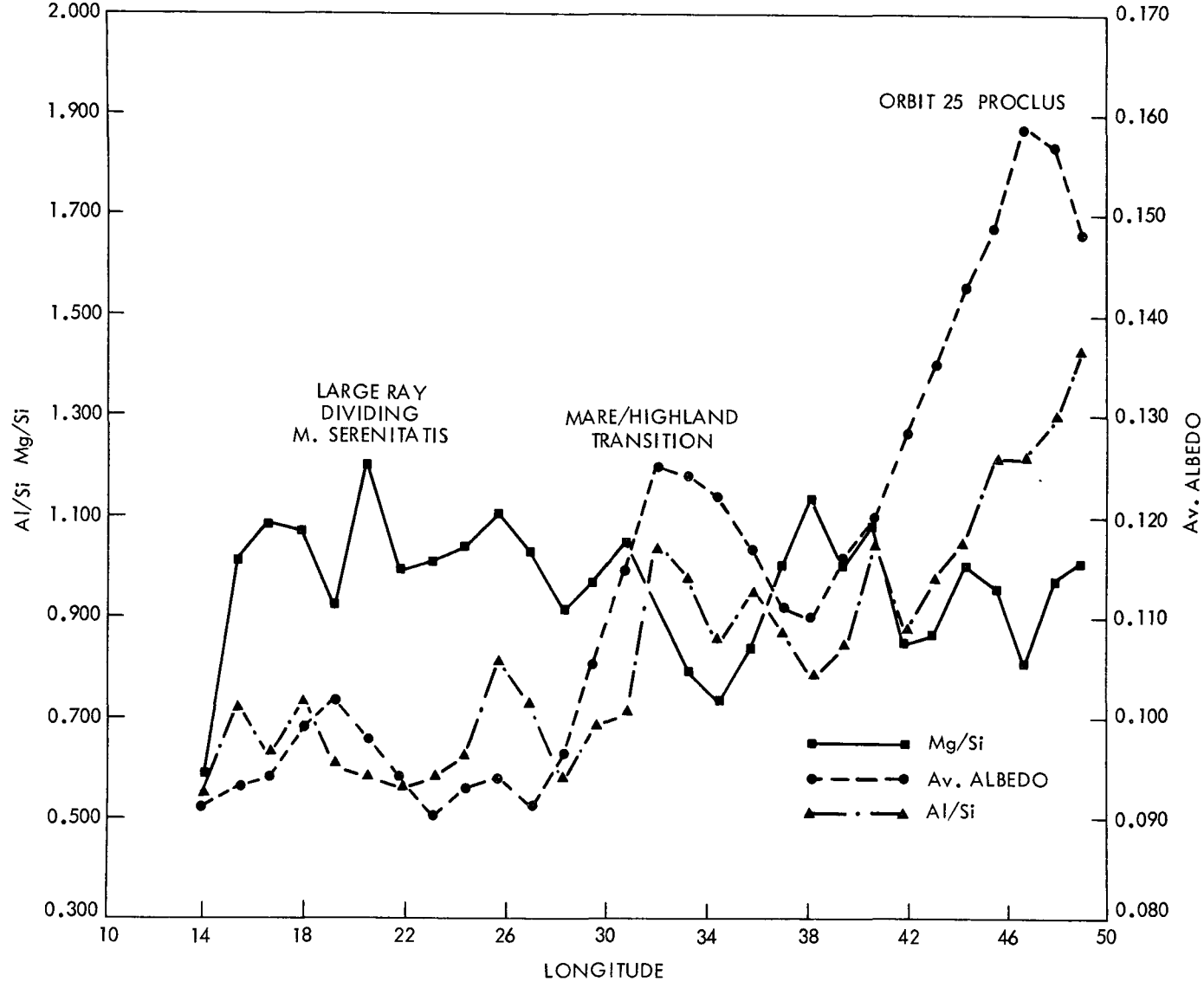

Figure 10. Intensity Ratios Compared to Optical Albedos along the Ground Track Corresponding to Orbit 72

A number of specific conclusions can be drawn about the composition of the lunar highlands. First, the x-ray intensity ratios, when reduced to composition ratios, suggest that the highland crust is broadly similar over very large areas. There are regional gradients apparent within the highlands; in particular, the near side highlands are somewhat lower in aluminum and higher in magnesium than those of the far side. This can be explained by at least two phenomena. First, there has undoubtedly been some ballistic transport of mare material into the near side highlands. Second, there are many small patches of mare material, mapped as Imbrium or Eratosthenian mare by Wilhelm and McCauley (1971), in the front side highlands along the flight path.

The higher proportion of aluminum in the highlands is probably due largely to a greater proportion of plagioclase. This conclusion is based on correlative data from other orbital experiments and from examination of thin sections of samples from Apollo 14 and 15. The gamma ray spectroscopy experiment shows that there is far too little ^{40}K in the highlands for the aluminum to be accounted for by alkali feldspar. Plagioclase, on the other hand, is abundant in most breccia samples from the Apennine Front and the Apollo 14 landing side, and widespread though scarce in the mare regolith. The higher albedo of the highlands appears to correlate well with aluminum content (Figures 9 and 10). The television pictures from Surveyor VII by Shoemaker et al. (1968) also showed several blocks on the north slope of Tycho that were originally interpreted as feldspar. Taken together, these several lines of evidence strongly indicate

plagioclase-rich highlands. However, the composition can not be due only to enrichment in plagioclase, relative to the mare rocks, at the expense of other minerals, because the magnesium content does not go down as aluminum content goes up. Petrologically, this suggests that the highlands were not formed by simple crystal fractionation of a basaltic magma whose residue was later erupted to form the maria (Wood et al. (1970)).

The question of what specific rock types comprise the highlands can not be answered fully at this time, but some inferences can be drawn. First, it is clear that the highlands are not dominantly anorthosite. This is shown by Table 1; the Al/Si ratio of the highlands are too low and the Mg/Si ratio too high. There are, of course, almost certainly local concentrations of anorthosite, such as that from which sample 15415 came; (Hollister et al. (1972)) suggest that this rock was formed by crystal fractionation of a gabbroic anorthosite magma. The relation if KREEP to the lunar highlands is still not clear. The Al/Si ratio of KREEP is not as high as that of most parts of the highlands (Figures 7 and 8). However, it does come close to that measured over the Apennine Mountains, which is of considerable interest in view of Myer's (1972) suggestion that the lower part of the highland crust (presumably exposed in the Apennines) is KREEP. Further speculation seems unwarranted until more highland samples are available.

When viewed with all other available information (summarized by Lowman (1972)), the x-ray data suggest that the dominant rock type of the lunar highlands

is a plagioclase-rich pyroxene-bearing rock, probably anorthositic gabbro or feldspathic basalt. Local occurrences of anorthosite are probable; small areas of granitic (in a chemical sense) rock may also occur. KREEP, as previously noted, may be significant constituent.

Turning to the maria, we see that the refined x-ray data do not support our earlier conclusion (Adler et al. 1972b) that there are systematic chemical differences between the irregular and circular maria. This does not invalidate Soderblom's (1971) work, but simply suggests that the differences, if real, are not such as can be detected by the S-161 experiment.

The Al/Si ratios of the maria as calculated from the x-ray intensities appear systematically higher and the Mg/Si ratios lower, than those of analyzed mare basalts. This effect is probably due to the fact that the x-ray fluoresence experiment is essentially a surface analyzer; it sees chiefly soils, and these have been shown to contain a substantial foreign component, perhaps from the highlands. Schnetzler, et al (1972), for example, show that soil 15531 could be formed by 88% 15555 basalt, 6% KREEP, and 6% plagioclase.

In summary, the main geologic conclusion from the S-161 experiment is that the moon appears to have a widespread differentiated crust (the highlands) systematically richer in aluminum and poorer in magnesium than the maria. The major rock type is probably chemically equivalent to anorthositic gabbro, with local areas of anorthosite and possibly KREEP and granitic rocks. This crust is pre-mare, probably between 4 and 4.6 billion years old. Its formation may represent the first major internal differentiation of the moon.

Table 1

Intensity Ratios and Corresponding Concentration Ratios of Al/Si and Mg/Si for the Various Features Overflown During the Apollo 15 Remote Sensing Geochemical Mapping Experiment

Feature	Intensity Ratios		N*	Concentration Ratios	
	Al/Si±1σ	Mg/Si±1σ		Al/Si±1σ	Mg/Si±1σ
W. of Diophantus and Delisle, NE of Schröters Valley	0.63±0.28	0.96±0.28	15	0.26±0.13	0.21±0.06
Mare Serenitatis	0.68±0.16	1.12±0.31	217	0.28±0.08	0.21±0.06
Diophantus and Delisle Area	0.69±0.20	1.16±0.35	15	0.29±0.10	0.26±0.07
Archimedes Rille Area	0.69±0.16	0.86±0.22	106	0.29±0.08	0.19±0.05
Mare Imbrium	0.71±0.21	0.95±0.28	159	0.30±0.10	0.21±0.06
Mare Tranquillitatis	0.81±0.13	1.15±0.21	170	0.34±0.06	0.25±0.04
Mare E. of Littrow (Maraldi)	0.83±0.16	0.99±0.21	29	0.35±0.08	0.22±0.04
Palus Putredinus	0.83±0.18	1.37±0.16	8	0.35±0.09	0.30±0.03
Mare Fecunditatis	0.84±0.12	1.13±0.17	101	0.36±0.06	0.25±0.03
Apennine Mts.	0.84±0.18	1.06±0.22	55	0.36±0.09	0.23±0.05
Haemus Mts., W. Border of Serenitatis	0.89±0.21	1.12±0.22	49	0.38±0.10	0.25±0.05
Mare Crisium	0.90±0.16	1.19±0.25	43	0.39±0.08	0.26±0.05
Tsiolkovsky	0.90±0.24	0.78±0.09	7	0.39±0.11	0.18±0.02
Haemus Mts., S+SW of Serenitatis	0.94±0.15	1.16±0.20	53	0.40±0.07	0.26±0.04
Littrow Area	0.98±0.22	1.13±0.30	51	0.42±0.10	0.25±0.06

Table 1 (continued)

Feature	Intensity Ratios		N*	Concentration Ratios	
	Al/Si±1σ	Mg/Si±1σ		Al/Si±1σ	Mg/Si±1σ
Mare Smythii	1.04±0.13	1.22±0.27	30	0.45±0.06	0.27±0.06
Taruntius Area, between Tranquillitatis and Fecunditatis	1.06±0.14	1.17±0.14	45	0.45±0.07	0.26±0.02
Langrenus Area, E. of Fecunditatis to 62.5°E	1.10±0.24	1.07±0.27	37	0.48±0.11	0.24±0.06
Highlands between Crisium + Smythii (Mare Spumans and Mare Undarum Area)	1.17±0.13	0.99±0.22	53	0.51±0.06	0.22±0.05
Highlands E. of Fecunditatis, Kapteyn Area 68-73°E 7.5-15°S	1.17±0.21	0.98±0.22	52	0.51±0.10	0.22±0.05
Highlands W. of Crisium	1.17±0.20	1.05±0.25	80	0.51±0.10	0.23±0.05
Highlands E. of Fecunditatis 62.5-68°E, 4-12.5°S	1.18±0.20	0.98±0.26	51	0.52±0.10	0.22±0.05
W. border of Smythii to 4-5° out from Rim	1.19±0.13	0.97±0.16	43	0.52±0.06	0.22±0.03
S. of Crisium, Apollonius Area, to Fecunditatis, 50-60°E	1.20±0.13	1.04±0.13	42	0.53±0.06	0.23±0.03
E. border of Crisium out to 6° from Rim	1.22±0.19	0.99±0.19	44	0.54±0.09	0.22±0.04
Tsiolkovsky - Rim	1.23±0.25	0.70±0.09	7	0.54±0.12	0.16±0.02
Highlands between Crisium and Smythii, 2.5°S 69°E, 5°S 76°E, 12°N 80°E, 10°N 83°E.	1.24±0.13	0.99±0.17	48	0.55±0.06	0.22±0.03

Table 1 (continued)

Feature	Intensity Ratios		N*	Concentration Ratios	
	Al/Si±1σ	Mg/Si±1σ		Al/Si±1σ	Mg/Si±1σ
Highlands W. of Tsiolkovsky, 110-124°E to 9-21°S	1.29±0.23	0.85±0.19	89	0.57±0.11	0.19±0.04
Highland E. of Fecunditatis 73-85°E, 10-19°S	1.30±0.28	0.95±0.24	70	0.58±0.13	0.21±0.05
S and SW of Sklodowska, 86-101°E, 18-23°S	1.33±0.29	0.86±0.33	59	0.59±0.14	0.19±0.07
Pirquet, 135-145°E, 18-23°S	1.33±0.32	0.72±0.23	46	0.59±0.15	0.16±0.05
E. border of Smythii, out to4-5°	1.34±0.20	0.92±0.17	37	0.60±0.10	0.21±0.03
Pasteur Hilbert Highlands area 101.5-110°E, 7-18°S	1.35±0.21	0.79±0.21	48	0.60±0.10	0.18±0.04
Hirayama, highlands E. of Smithyii, 89°E 12°S, 100°E 15°S, 98°E 2°S, 103°E 5°S	1.39±0.15	0.86±0.18	63	0.62±0.07	0.19±0.04
Highlands around Tsiolkovsky	1.40±0.26	0.71±0.30	39	0.62±0.12	0.15±0.06
S. Part of Gagarin, 144-153°E, 21-23°S	1.45±0.50	0.69±0.22	22	0.65±0.24	0.14±0.05
Al/Si and Mg/Si Concentration Ratios of Selected Lunar Samples					
Apollo 12, Oceanus Procellarum Average of Type AB Rocks (a)				0.22	0.22
Apollo 15, Hadley Apennines Average of Rocks (b)				0.22	0.27
Apollo 12, Oceanus Procellarum, Type B Rocks, Average (a)				0.22	0.37

Table 1 (continued)

Feature	Intensity Ratios		N*	Concentration Ratios	
	Al/Si±1σ	Mg/Si±1σ		Al/Si±1σ	Mg/Si±1σ
Apollo II, Mare Tranquillitatis, High K Rocks - Average (c)				0.23	0.24
Apollo 12, Oceanus Procellarium, Type A Rocks - Average (a)				0.24	0.31
Rock 12013 (a)				0.24-0.30	0.20
Apollo II, Mare Tranquillitatis, Average of low K Rocks (c)				0.29	0.23
Dark of Rock 12013 (d,e,f)				0.33	0.22
Apollo 12, Oceanus Procellarium Average of Soils (a)				0.33	0.29
Surveyor VI, Sinus Medii, Regolith (g, h)				0.34	0.20
Apollo 15, Hadley-Apennines, Soils (b)				0.34	0.30
Surveyor V, Mare Tranq. Regolith (i,h)				0.35	–
Luna 16, Mare Fedunditatis, Rocks (j)				0.35	0.21
Apollo 11, Mare Tranquillitatis, Bulk Soils Average (c)				0.37	0.24
Apollo 14, Fra Mauro, Average of Rocks (k)				0.38	0.26

Table 1 (continued)

Feature	Intensity Ratios		N*	Concentration Ratios	
	Al/Si±1σ	Mg/Si±1σ		Al/Si±1σ	Mg/Si±1σ
Kreep Average (d,e,f)				0.39	0.21
Apollo 14, Fra Mauro, Soils (k)				0.41	0.26
Norite Material, Average (l,m)				0.42	0.20
Luna 16, Mare Fecunditatis, Bulk Soils (j)				0.42	0.27
Surveyor VII, Rim of Tycho, Regolith (n,h)				0.55	0.20
Anorthositic Gabbros, Apollo 11 and 12 (l,m)				0.64	0.21
Rock 15418, Apollo 15, Gabbroic Anorthosite (b)				0.67	0.15
Gabbroic Anorthosites, Apollo 11 and 12 (l,m)				0.82	0.074
Anorthosites, Apollo 11 and 12 (l,m)				0.89	0.038
Rock 15415, Apollo 15, Anorthosite Genesis Rock (b)				0.91	0.003

N* is the number of individual data points used to determine the average Al/Si and Mg/Si values ±1 standard deviation and was obtained from the various passes over each feature.

[a]Proceedings of the Second Lunar Science Conference (1971)
[b]LSPET (1972)
[c]Proceedings of the Apollo 11 Lunar Science Conference (1970)
[d]McKay et al. (1971)
[e]Meyer et al. (1971a)
[f]Meyer et al.(1971b)
[g]Turekevich et al. (1968a)
[h]Mason and Melson (1970)
[i]Turekevich et al. (1967)
[j]Vinogradou (1971)
[k]LSPET (1971)
[L]Wood et al. (1971)
[M]Marvin et al. (1971)
[N]Turkevich et al. (1968b)

REFERENCES

Adler I., Trombka J., Gerard J., Schmadebeck R., Lowman P., Blodget H., Yin L., Eller E., Lamothe R., Gorenstein P., Bjorkholm P., Harris B. and Gursky H. (1972a) X-ray Fluorescence Experiment, In Apollo 15 Preliminary Science Report, in Press.

Adler I., Trombka J., Gerard J., Lowman P., Schmadebeck R., Blodget H., Eller E., Yin L., Lamothe R., Gorenstein P. and Bjorkholm P. (1972b) Apollo 15 Geochemical X-ray Fluorescence Experiment: Preliminary Report, Science 175, 436-440.

Gold T. (1966) The Moon's Surface, In the Nature of the Lunar Surface (editors Wilmon N. Hess, Donald H. Menzel and John A. O'Keefe), pp. 107-121, The John Hopkins Press.

Gold T., The Depth of the Lunar Dust Layer (abstract), "Revised Abstracts of the Third Lunar Science Conference," p. 321, January 1972.

Hollister L., Trzcienski W. Jr., Dymek R., Kulick C., Weigand P. and Hargraves R., Igneous Fragment 14310, 21 and the Origin of the Mare Basalts (abstract), "Revised Abstracts of the Third Lunar Science Conference," p. 386, January 1972.

Lowman Paul D. Jr. (1972), The Geologic Evolution of the Moon, Jour. of Geol., in Press.

LSPET (Lunar Sample Preliminary Examination Team) (1971) Preliminary Examination of Lunar Samples from Apollo 14, Science 173, 681-693.

LSPET (Lunar Sample Preliminary Examination Team) (1972) The Apollo 15 Lunar Samples: A Preliminary Description, Science 175, 363-375.

Marvin, U. B., Wood J. A., Taylor G. J., Reid J. B., Jr., Powell B. N., Dickey J. S., Jr., and Bower J. F. (1971) Relative Proportions and Probable Sources of Rock Fragments in the Apollo 12 Soil Samples, Proc. Second Lunar Sci. Conf., Geochim. Cosmochim. Acta Suppl. 2, Vol. 1, pp. 679-699. MIT Press.

Mason B. H and Melson W. G. (1970) The Lunar Rocks, p. 11, Wiley.

McKay, D. S., Morrison D. A., Clanton U. S., Ladle G. H. and Lindsay J. F. (1971) Apollo 12 Soil and Breccia, Proc. Second Lunar Sci. Conf., Geochim. Cosmochim. Acta Suppl. 2, Vol. 1, pp. 755-773, MIT Press.

Meyer, C., Jr., Aitken F. K., Brett R., McKay D. S. and Morrison D. A. (1971a) Rock Fragments and Glasses Rich in K, REE, P in Apollo 12 Soils: Their Mineralogy and Origin. Unpublished Proc. of the Second Lunar Sci. Conf., Houston, January, 1971.

Meyer C. Jr., Brett Robin, Hubbard N. J., Morrison D. A., McKay D. S., Aitken F. K., Takeda H. and Schonfeld E. (1971b) Mineralogy, Chemistry, and Origin of the KREEP Component in Soil Samples from the Ocean of Storms, Proc. of the Second Lunar Sci. Conf., Geochim. Cosmochim. Acta Suppl. 2, Vol. 1, pp. 393-411.

Meyer Charles Jr., Mineral Assemblages of Lithic Fragments of Non-Mare Lunar Rock Types (abstract) "Revised Abstracts of the Third Lunar Science Conference," p. 542, January, 1972.

Proc. of the Apollo 11 Lunar Sci. Conf. (1970) Geochim. Cosmochim. Acta Suppl. 1, Vol. 1-3. Pergamon.

Proc of the Second Lunar Sci. Conf. (1971) Geochim. Cosmochim. Acta Suppl. 2, Vol. 1-3, MIT Press.

Schnetzler C. C., Philpotts John A., Nava David F., Schuhmann Shuford, Thomas Herman H. (1972) Geochemistry of Apollo 15 Basalt 15555 and Soil 15531, Science 175, 426-428.

Shoemaker E. M., Batson R. M., Holt H. E., Morris E. C., Rennilson, J. J. and Whitaker E. A. (1968) Television Observations from Surveyor VII. In Surveyor VII: A Preliminary Report, NASA SP-173, pp. 13-81 Office of Tech. Utilization Washington, D.C.

Soderblom L. A. (1970) The Distribution and Relative Ages of Regional Lithologies in the Lunar Maria (abstract), "Abstracts with Programs V. 2, No. 70, Geological Society of America," p. 690-691, 1970 Annual Meeting.

Turkevich A. L., Franzgrote E. J. and Patterson J. H. (1967) Chemical Analysis of the Moon at the Surveyor 5 landing site: Preliminary Results. Science 158, 635-637.

Turkevich A. L., Patterson J. H. and Franzgrote E. J. (1968a) Chemical Analysis of the Moon at the Surveyor 6 Landing Site. Science 160, 1108-1110.

Turkevich A. L., Franzgrote E. J. and Patterson J. H. (1968b) Chemical Analysis of the Moon at the Surveyor 7 Landing Site: Preliminary Results. Science 162, 117-118.

Vinogradov A. P. (1971) Preliminary Data on Lunar Ground Brought to Earth by Automatic Probe "Lunar-16," Proc. of the Second Lunar Sci. Conf., Geochim. Cosmochim. Acta Suppl. 2, Vol. 1, pp. 1-16.

Wilhelms D. E. and McCauley J. F. (1971) Geologic Map of the Front Site of the Moon, U. S. Geological Survey, Washington, D.C.

Wood J. A., Dickey J. S., Jr., Marvin U. B., and Powell B. N. (1970) Lunar Anorthosites and a Geophysical Model of the Moon, Proc. Apollo 11, Lunar Sci. Conf., Geochim. Cosmochim. Acta Suppl. 1, Vol. 1, pp. 965-988. Pergamon.

Wood, J. A., Marvin U., Reid J. B., Taylor, G. J., Bowen J. F., Powell B. N. and Dickey J. S., Jr. (1971) Relative Proportions of Rock Types and Nature of the Light-Colored Lithic Fragments in Apollo 12 soil samples, unpublished Proc. of the Second Lunar Sci. Conf., January, 1971.